Steel and Composite Structures, *Vol. 36, No. 2 (2020) 187-196*
DOI: https://doi.org/10.12989/scs.2020.36.2.187

Experimental compressive behavior of novel composite wall with different width-to-thickness ratios

Ying Qin*, Xin Chen, Xing-Yu Zhu, Wang Xi and Yuan-Ze Chen

Key Laboratory of Concrete and Prestressed Concrete Structures of Ministry of Education, School of Civil Engineering, Southeast University, Nanjing, China

(*Received November 16, 2019, Revised June 7, 2020, Accepted July 7, 2020*)

Abstract. Double skin composite wall system owns several structural merits in terms of high load-carrying capacity, large axial stiffness, and favorable ductility. A recently proposed form of truss connector was used to bond the steel plates to the concrete core to achieve good composite action. The structural behavior of rectangular high walls under compression and T-shaped high walls under eccentric compression has been investigated by the authors. Furthermore, the influences of the truss spacings, the wall width, and the faceplate thickness have been previously studied by the authors on short walls under uniform compression. This paper experimentally investigated the effect of width-to-thickness ratio on the compressive behavior of short walls. Compressive tests were conducted on three short specimens with different width-to-thickness ratios. Based on the test results, it is found that the composite wall shows high compressive resistance and good ductility. The walls fail by local buckling of steel plates and crushing of concrete core. It is also observed that width-to-thickness ratio has great influence on the compressive resistance, initial stiffness, and strain distribution across the section. Finally, the test results are compared with the predictions by modern codes.

Keywords: width-to-thickness ratio; double skin composite wall; truss connector; compressive behavior

1. Introduction

Double skin steel-concrete composite wall has been increasingly used in high-rise buildings, safety-related facilities in the third generation of nuclear power plants, and future small modular reactor plants due to its merits of high load-carrying capacity, large axial stiffness, and favorable ductility compared with steel plate shear wall (Liu *et al.* 2018, Curkovic *et al.* 2019, Deng *et al.* 2019, Seddighi *et al.* 2019, Shariati *et al.* 2019) and reinforced concrete wall (Beiraghi 2018). The steel plates serve as the formwork when concrete is pouring. Meanwhile, the concrete core provides restraint to steel plates and prevents the inward buckling (Li *et al.* 2016). Composite action between steel plate and concrete core is largely achieved by employing cohesive bonding materials and different mechanical connectors such as headed studs (Yang *et al.* 2016, Bruhl and Varma 2017, Yan *et al.* 2018), Bi-steel connectors (McKinley and Boswell 2002), embedded shear bars (Eom *et al.* 2009), J-hook connectors (Huang and Liew 2016), connecting bolts (Luo *et al.* 2015), bi-directional corrugated-strip-core system (Leekitwattana *et al.* 2011), L-shaped and C-shaped connectors (Chen *et al.* 2019), combined diaphragm, distributed batten plates and transverse stiffeners (Nie *et al.* 2013, Chen *et al.* 2015, Huang *et al.* 2018), and enhanced C-channel connectors (Yan *et al.* 2019). In this research, a recently developed steel truss connectors were used to bond the steel plates and the concrete core to form an integrated component (Qin *et al.* 2019a). The steel truss connectors shown in Fig. 1 not only prevent separation of steel plates from concrete, but also offer shear resistance against longitudinal slip at the steel-concrete interface.

Extensive studies have been conducted on double skin profiled steel sheet composite wall system. It was firstly proposed by Wright (1998) from the concept of composite slab. Many researchers have performed various tests to evaluate the structural behavior of the wall under different loading such as axial compression (Hossain *et al.* 2015), cyclic loading (Dan *et al.* 2011), and combined compression and bending (Ridha *et al.* 2019).

Most research on double skin flat steel sheet composite walls focused on seismic behavior. Nie *et al.* (2013) performed cyclic tests on twelve composite walls and proposed a strength prediction approach based on the section analysis method. Chen *et al.* (2015) conducted a series of tests to study the response of double skin composite walls under cyclic loading. The effects of axial load ratio and the ratio of the tie bar spacing to steel plate thickness were investigated. Flexure-dominated behavior through cantilever action was found for wall specimens with large height-to-width ratio. Nguyen and Whittaker (2017) presented a numerical study of composite wall under reversed cyclic loading using the general purpose finite element program ABAQUS. It was found that the contribution of steel plates to the total shear resistance of the wall ranged from 20% to 70%, with varied faceplate slenderness ratio, reinforcement ratio, story drift, and level of damage. Ji *et al.* (2017) presented the experimental and

*Corresponding author, Associate Professor
E-mail: qinying@seu.edu.cn

http://www.techno-press.org/?journal=scs&subpage=8

ISSN: 1229-9367 (Print), 1598-6233 (Online)

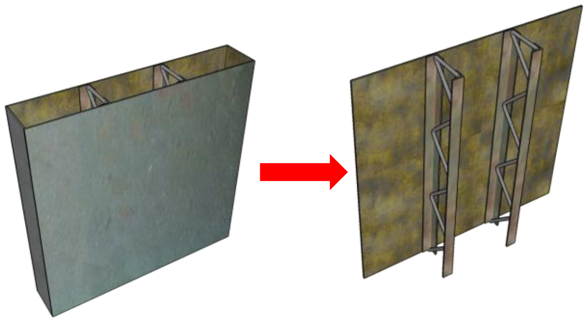

Fig. 1 Composite wall with steel truss connectors

numerical results to evaluate the cyclic in-plane shear behavior of composite wall with different reinforcement ratios and axial force ratio. The investigation demonstrated that axial compression did not obviously affect the shear strength but decreased the shear deformation capacity. Huang *et al.* (2018) tested five composite walls under constant axial compressive force and lateral reversed cyclic loading. The experimental results indicated that the wall specimens exhibited plentiful hysteresis performance, satisfactory ductility, and great energy dissipation capacity. Chen *et al.* (2019) evaluated the influence of low axial compression ratio and spacing-to-thickness ratio on the seismic behavior of composite wall. The formulas to predict the load-carrying capacity were established. To better investigate the dynamic behavior of structures, incremental dynamic analysis (Asgarian *et al.* 2012) and endurance time analysis (Hariri-Ardebili *et al.* 2014) has been proposed.

It should be noted that, besides the idea to use the composite wall itself to resist the earthquake as mentioned above, some other components were also promising to be applied in composite wall system to carry the cyclic loading. Frictional damper used the friction mechanism to dissipate the dynamic energy (Mirtaheri *et al.* 2011). Samani *et al.* (2014, 2015) investigated the effects of dynamic loading and various slippage loading on cyclic behavior of frictional dampers. Buckling-restrained brace was another alternative to be used (Gheidi *et al.* 2011, Mirtaheri *et al.* 2018). Furthermore, the technology of base isolation (Karami-Mohammadi *et al.* 2019) has been shown to be effective in preventing the structural damage during an earthquake.

Experimental studies on double skin composite walls under axial compression have been conducted by several researchers. Mydin and Wang (2011) and *Prabha et al.* (2013) presented the results of experimental and analytical investigation on the structural behavior of composite wall with lightweight foamed concrete. The load-carrying capacity of the wall was calculated using either the effective width method for steel sheets or the observed failure mode. Choi *et al.* (2014) described the compressive behavior of composite wall with shear studs connectors using ordinary and eco-oriented cement concrete. Simplified method to evaluate the buckling stress of steel plate was proposed based on test results. Hilo *et al.* (2016) developed a finite element model to simulate the axial load behavior of composite wall with embedded cold-formed steel (ECFS) tube. Comprehensive parametric studies were performed to evaluate the effects of the number of the ECFS, ECFS thickness, and ECFS shapes on the load resisting performance.

Previous compressive tests showed that the steel plates in composite wall with shear studs may experience premature local buckling even when the level of axial compression is still low. This means the point restraints provided by the shear studs to the steel plate are not strong enough to prevent the steel plate to separate from concrete core. Furthermore, severe damage was found at the location where shear studs were arranged. The test results from Yang *et al.* (2016) showed that the steel faceplates suffered from outward buckling around the wall at certain height. As has been seen from the test observation in previous research by the authors, the new proposed truss connectors were able to provide sufficient restraint and the steel faceplates only buckled between the adjacent trusses. Consequently, steel truss connectors can overcome the disadvantage mentioned above. As shown in Fig. 1, steel trusses are welded to the internal surface of steel plates by automatic machines. The size of truss can be adjusted according to the thickness of composite wall. The well-constructed steel truss connectors provide an interlocking effect on external steel plates when the steel plates tend to buckle outwards under axial compression.

Before such composite walls can be applied in practice, it is of importance to assess the structural behavior in terms of failure modes, ultimate strength, and axial stiffness. Qin *et al.* (2019a, 2019b) have investigated the structural behavior of high walls under compression. Furthermore, the influences of truss spacing, wall width, faceplate thickness on the compressive behavior of short walls have been studied (Qin *et al.* 2020a, 2020b). In this paper, the compressive behavior of the proposed double skin composite wall with different width-to-thickness ratios was investigated. A series of compressive tests were performed to evaluate the influence of the width-to-thickness ratio on the structural behavior of the composite wall. Finally, the capacity predictions by several modern codes were compared and discussed.

2. Experimental program

2.1 Test specimens

The test program consists of three double skin composite walls with steel truss connectors, i.e., W-150, W-175, and W-200. Each specimen is composed of two external steel plates, concrete core, steel truss connectors, and bottom endplate. Fig. 2 and Table 1 show the configuration details of all specimens. The composite walls were designed to behave as short walls to eliminate global buckling with an overall height of 500 mm. The width was selected as 900 mm, which led to the height-to-width ratio of 0.56. The thickness was selected as 150 mm, 175 mm, and 200 mm, respectively. The corresponding width-to-thickness ratio was 6.0, 5.1, and 4.5, respectively. The thickness of steel plates was 4 mm. A cover plate was

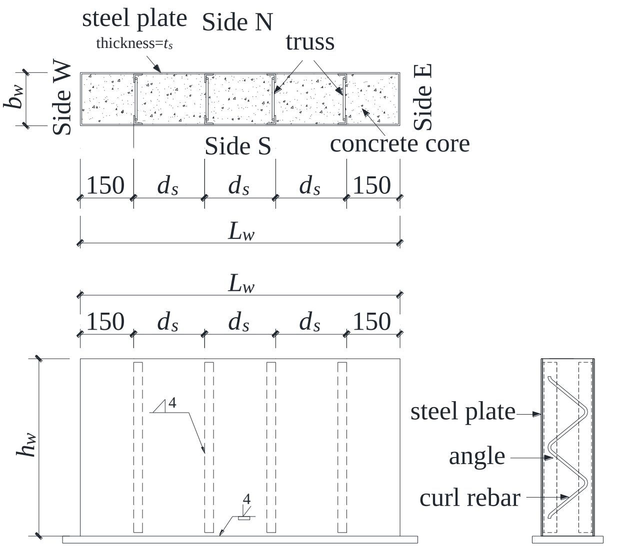

Fig. 2 Details of test specimens (dimension in mm)

Table 1 Specimen details

Specimen No.	h_w	L_w	b_w	t_s	d_s
	mm	mm	mm	mm	mm
W-150	500	900	150	4	200
W-175	500	900	175	4	200
W-200	500	900	200	4	200

Note: h_w, L_w and b_w are the height, width and thickness of sandwich composite wall; t_s is the thickness of steel plate; and d_s is the truss spacing

welded to the bottom of the wall specimen in order to apply uniform loading. The dimension of the truss was determined by preliminary finite element modelling (Qin *et al.* 2020a). The truss connector consisted of curl rebar with the diameter of 8 mm serving as web member and two angles with the dimension of L40×40×4 serving as chord members. JGJ/T 380-2015 (2015) requires that the spacing-to-thickness ratio should be less than $60\sqrt{235/f_y}$ for walls with T-shaped stiffeners. Since the structural behavior of truss connectors is believed to be similar to that of T-shaped stiffeners, the spacing-to-thickness ratio in this research was taken as $50\sqrt{235/f_y}$, and the corresponding truss spacing was 200 mm.

2.2 Material properties

Grade Q235 mild steel plates were employed in all specimens which were manufactured in Zhejiang Southeast Space Frame Group Company Limited in China. To obtain the material properties of the steel plates in tension, three 20 mm width coupons were cut and fabricated from the same batch of steel in accordance with GB/T 2975-2018 (2018) and tested in accordance with GB//T 228.1-2010 (2010). The elastic modulus, yield strength, and ultimate strength were 1.99×10^5 MPa, 346.0 MPa, and 364.8 MPa, respectively.

Fig. 3 Test setup

Grade C20 concrete was used in the experiments. Three 150 mm cubes were cast and cured in environments similar to that of the test walls in order to obtain the compressive strength of concrete. The tested cubic compressive strength under the requirement of GB/T 50081-2002 (2002) was 23.9 MPa, and the corresponding cylinder strength was 16.0 MPa according to GB 20010-2010 (2010). It should be noted that low concrete strength was selected in this research. This is due to the limitation of loading capacity of test machine. However, the influence of concrete strength is limited on the studied purpose in this research.

2.3 Test setup

All composite walls were tested under axial compression with a 10000 kN testing machine in Southeast University, as shown in Fig. 3. Each specimen was placed in the rig to ensure that the loading point and centroid coincide. The test was proceeded in a load-controlled manner. The load interval was 500 kN and the load was maintained to record the data and observe the test phenomenon. Each specimen was loaded to failure until the load-carrying capacity had dropped to 80% of ultimate capacity.

2.4 Instrumentations

The arrangement of linear variable displacement transducers (LVDTs) was presented in Fig. 4. Four LVDTs (D1-D4) were fixed at the bottom of the walls to monitor the axial shortening of the walls. Additional six LVDTs (D5-D10) were horizontally placed to record the out-ofplane deformation. A total of fourteen strain gauges were bonded to the surfaces of steel plates at mid-height cross-section, and the locations were illustrated in Fig. 5.

3. Experimental results and analysis

3.1 Failure modes

Fig. 6 shows the failure modes of the tested three specimens. Two types of failure modes were observed in the tests, i.e., local buckling of steel plates, and concrete crushing. Global buckling of the entire composite wall was not found in the tested short walls. It can also be found from Fig. 6 that the locations of local buckling differed on two side of steel plates in all specimens.

For Specimen W-150, the steel plates near the top of wall started to buckle on both sides S and N as W-150 reached its ultimate resistance, as shown in Figs. 6(a) and 6(b). Local buckling continued to develop as the load progressed to drop. For Specimen W-175, as the load increased to 85% of ultimate resistance, local buckling started to develop on side S. As the load reached 96% of the ultimate resistance, similar buckling was found on side N.

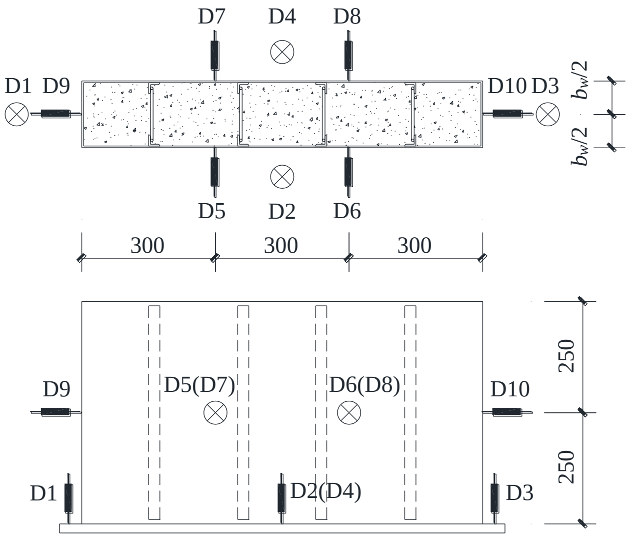

Fig. 4 Arrangement of LVDTs

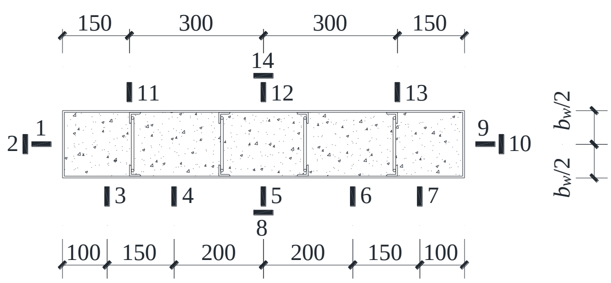

Fig. 5 Arrangement of strain gauges

(a) Specimen W-150 (side S)

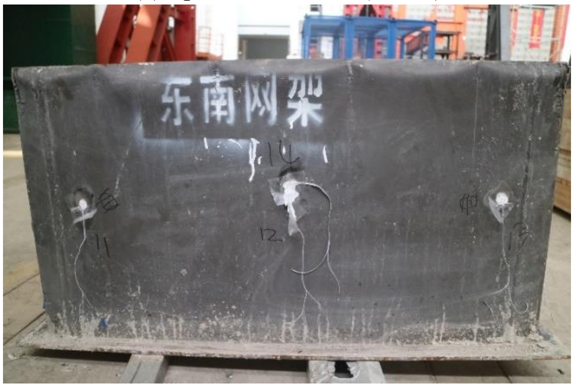

(b) Specimen W-150 (side N)

(c) Specimen W-175 (side S)

(d) Specimen W-175 (side N)

Continued-

(e) Specimen W-200 (side S)

(f) Specimen W-200 (side N)

Fig. 6 Failure modes

The failure of W-175 was shown in Figs. 6(c) and 6(d). For Specimen W-200, local buckling started to develop in the steel plates at the top of side N as the specimen achieved 91% of its ultimate resistance. The buckling progressed to the bottom of side S as the axial compression continued the increase. W-200 finally failed by concrete crushing, as shown in Figs. 6(e) and 6(f).

3.2 Axial compressive behavior

Load-axial shortening curves for three specimens are plotted in Fig. 7. All specimens show similar load versus axial shortening performance, which is consistent with previous observations (Qin *et al.* 2020a, b). In the first stage, the curves stably go up before the steel plates start to buckle. The behavior of composite wall is completely elastic and the steel plates work compositely with the concrete core through the truss connectors. In the second stage, local buckling slowly develops in steel plates, and the slope of curves gradually decreases. After approaching the ultimate resistance, the buckling becomes more severe. Meanwhile, the concrete crushing is developing in the specimens. The curves begin to go down with the increase in axial shortening due to the cumulative damage in the specimens.

3.3 Buckling stress

The buckling stress is essential to evaluate the behavior of steel plates in composite wall. From test observation

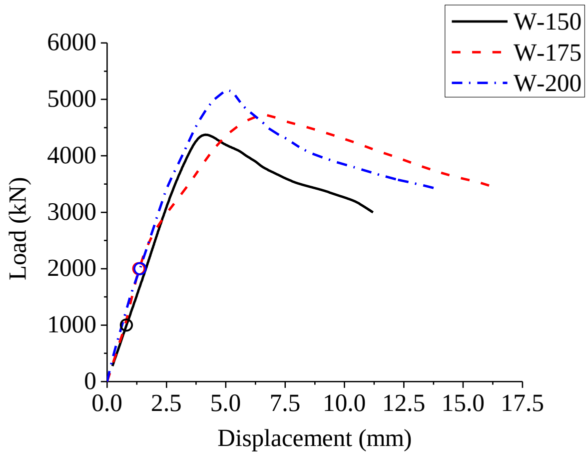

Fig. 7 Load-axial displacement curves

shown in Fig. 6, local buckling gradually developed in the thin steel plates in double skin composite walls when the walls were under compressive loading. As the steel plates are in rigid contact with concrete core, they can only buckle outwards. Meanwhile, the steel trusses provide restraint to the steel plates along the wall height and thus, buckling is normally found between the two adjacent truss connectors. In order to obtain the buckling strain and the corresponding buckling stress and buckling load, strain gauges were arranged at the surface of the steel plates. During the elastic stage, the strains are expected to increase linearly with the growth of axial loading. When the plastic deformation starts to develop, the strains at the buckling location are expected to change abruptly.

Fig. 8 shows the partially-enlarged drawing of load-strain curves of typical points for three specimens. The points where strain values start to change are marked by red squares. It can be seen from Fig. 8(a) that the buckling strain for Specimen W-150 is 365 $\mu\varepsilon$, and the corresponding buckling stress and buckling load are 72.6 MPa and 1000 kN, respectively. Fig. 8(b) shows that Specimen W-175 has a buckling strain of 568 $\mu\varepsilon$, and the corresponding buckling stress and buckling load are 113.0 MPa and 2000 kN, respectively. As can be found from Fig. 8(c), for Specimen W-200, the buckling strain, buckling stress, and buckling load are 395 $\mu\varepsilon$, 78.6 MPa, and 2000 kN, respectively.

3.4 Ultimate resistance and axial stiffness

The ultimate resistance N_u and the corresponding axial shortening d_u of all tested wall specimens were given in Table 2. The ultimate resistance of Specimens W-175 and W-200 are 6.7% and 15.6%, respectively, higher than that of Specimen W-150. The growth in ultimate resistance was largely due to the contribution from additional concrete area. Meanwhile, it can be found that the increase rate of resistance was higher than the increase rate of concrete area. As can be seen from Fig. 2 that there are more steel trusses in Specimen W-200 than in Specimen W-175, it is indicated that truss connectors contribute to the load-carrying capacity of composite wall. The initial stiffness is calculated by the ratio of $0.3N_u$ to the corresponding axial shortening

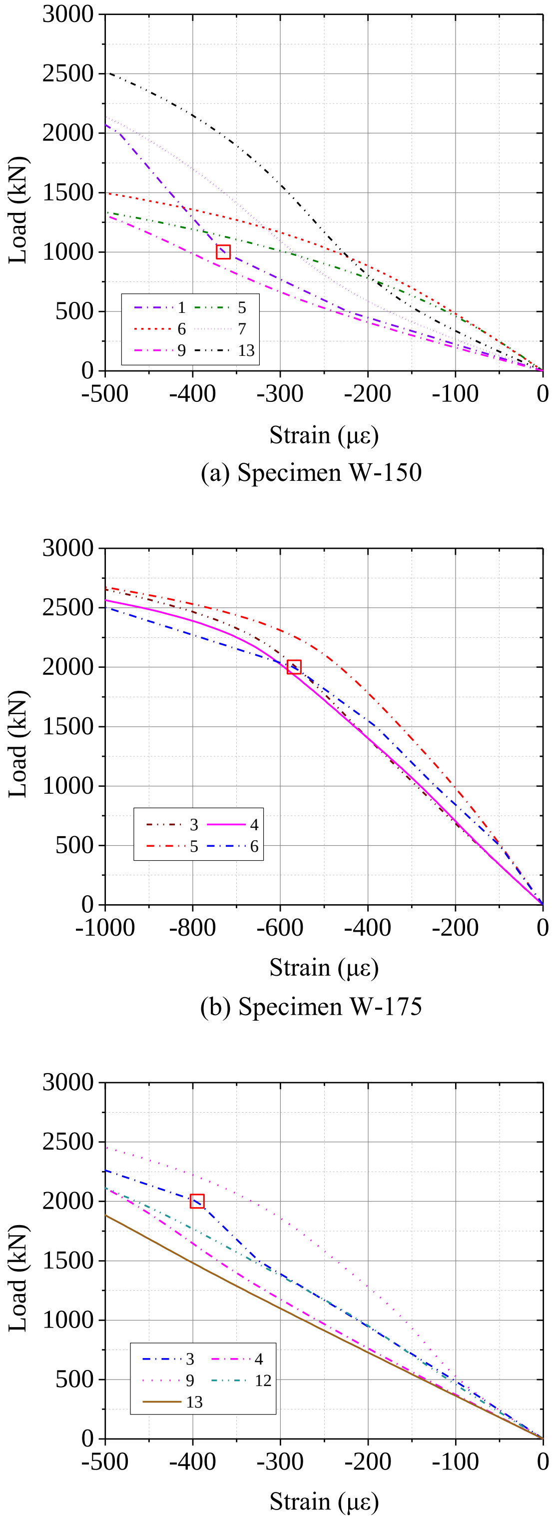

(a) Specimen W-150

(b) Specimen W-175

(c) Specimen W-200

Fig. 8 Determination of buckling strain

$d_{0.3u}$. The calculated initial stiffness for Specimens W-150, W-175, and W-200 are 1220 kN/mm, 1493 kN/mm, and 1556 kN/mm, respectively. The initial stiffness of Specimens W-175 and W-200 are 22.4% and 27.5%, respectively, higher than that of Specimen W-150.

Table 2 Test results

Specimen	N_b	d_b	N_u	d_u	$d_{0.3u}$	$d_{0.8u}$	K_b	$K_{0.3u}$
	kN	mm	kN	mm	mm	mm	kN/mm	kN/mm
W-150	1000	0.82	4500	4.02	1.11	2.96	1217	1216
W-175	2000	1.34	4800	6.65	1.02	3.99	694	806
W-200	2000	1.39	5200	5.09	1.00	3.35	1104	1109

Table 2 also gives the buckling load (N_b) and the corresponding axial shortening (d_b), the axial shortening corresponding to $0.3N_u$ ($d_{0.3u}$), and the axial shortening corresponding to $0.8N_u$ ($d_{0.8u}$). The buckling points for three specimens were marked in Fig. 7 by circles at the lower portion of the curves. It can be seen that the slope of curves does not change significantly after the local buckling of steel plates. This means that local buckling does not obviously affect the axial stiffness of the wall. This is also consistent with the observation previously (Qin *et al.* 2020a, 2020b).

In order to further quantify the effect of buckling on axial stiffness, two kinds of secant stiffness (K_b and $K_{0.3u}$) were used (Qin *et al.* 2020a), as shown in Fig. 9. K_b uses the buckling point as the starting point and the $0.8N_u$ point as the terminal point, as expressed by Eq. (2). While $K_{0.3u}$ uses the $0.3N_u$ point as the starting point and the $0.8N_u$ point as the terminal point, as expressed by Eq. (3). The calculated secant axial stiffness was given in Table 2. It can be found that unlike the trend in initial axial stiffness which goes up with the increase in wall thickness, the secant axial stiffness shows no obvious trend. Specimen W175 has the lowest secant axial stiffness. This is because plastic deformation develops more quickly in this specimen after buckling of steel plates. Meanwhile, it can be observed that the two types of secant stiffness for Specimens W-150 and W-200 exhibit no obvious differences, while slight differences were found for Specimen W-175.

$$K_b = \frac{0.8N_u - N_b}{d_{0.8u} - d_b} \tag{1}$$

$$K_{0.3u} = \frac{0.8N_u - 0.3N_u}{d_{0.8u} - d_{0.3u}} \tag{2}$$

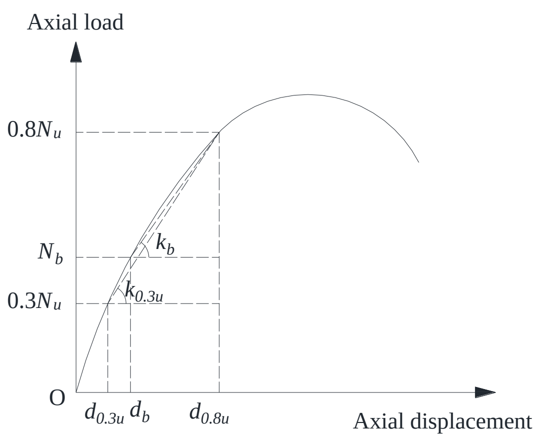

Fig. 9 Determination of secant stiffness

3.5 Ductility ratio and strength index

Ductility ratio is used to evaluate the ability of wall to undergo large plastic deformation without severe loss of resistance (Qin *et al.* 2020a, b). It can be calculated by the ratio of the axial shortening corresponding to 85% of the ultimate resistance during the recession stage ($d_{0.85u}$) to the axial shortening corresponding to ultimate resistance (d_u), as shown in Eq. (4). The calculated ductility ratios for Specimens W-150, W-175, and W-200 are 1.65, 1.73, and 1.37, respectively. It can be observed that the ductility ratio for Specimens W-150 and W-175 are similar, while Specimen W-200 has the poorest ductility. This is because the restraint provided by truss connectors becomes weaker as the wall becomes thicker. The dimension of the truss connectors should be enlarged with the increase in wall thickness.

$$\mu=\frac{d_{0.85u}}{d_u} \tag{4}$$

Strength index (SI) is used to evaluate the utilization of cross-sectional resistance of the composite wall. It can be calculated by the ratio of the ultimate resistance in the test (N_u) to the fully-utilized cross-sectional resistance (N_f) (Qin *et al.* 2020a, b). The expression is given by Eq. (5). The calculated strength index for Specimens W-150, W-175, and W-200 are 0.92, 0.90, and 0.90, respectively. It can be observed that the strength index does not change noticeably with the change in wall thickness. Meanwhile, the values of strength index for all specimens are smaller one. This is because yield strength rather than the buckling strength of steel plates is used to calculate the fully-utilized cross-sectional resistance, which overestimates the contribution from steel. It should be noted that the cylinder compressive strength is used for concrete in the calculation.

$$SI=\frac{N_u}{N_f}=\frac{N_u}{f_yA_s+f_cA_c} \tag{5}$$

3.6 Load-lateral deformation responses

The responses between the axial load and the lateral deformation were shown in Fig. 10. It can be seen that in the elastic stage, the lateral deformation of composite wall is quite small. It gradually climbs up as the axial loading progresses. After the buckling of steel plates, the lateral deformation grows up more quickly. The lateral deformation rapidly develops after the ultimate resistance has been achieved. This indicates that most of the local buckling of steel plates occurs after the specimen reaches its load-carrying capacity.

3.7 Load-strain responses

The strain distribution under each loading level is shown in Fig. 11. The yield strain is 1739 $\mu\varepsilon$ and is plotted in Fig. 11 by red dash line. It can be seen that at the beginning of loading, the strain is mostly distributed uniformly across the wall section. The strain distribution becomes non-uniform before the steel reaches its yield strength. This is because local buckling occurs earlier than yielding, which causes the stress and strain to be rearranged in the wall section. As the load continues to grow, the increase rate of strain becomes greater. At the end of the test, the strains at different locations differ significantly. It can also be found that under the same loading level, the strain in Specimen W-150 is the highest, while that in Specimen W-200 is the lowest. This is expected as the concrete core in thicker wall carries more axial load. Meanwhile, the strain is more uniform in specimen with greater thickness.

4. Code-based design

AISC 360-16 (2016), Eurocode 4 (EN 1994-1-1, 2004) and CECS 159 (2004), respectively, provide the calculation method to predict the compressive resistance of composite members. All these modern codes consider the load-carrying capacity of the composite wall as the summation of the contributions from both steel and concrete. AISC 360-16 (2016) assumes the steel reaches its buckling strength f_{cr} while concrete reaches 70% of its compressive strength, which can be expressed by Eq. (6).

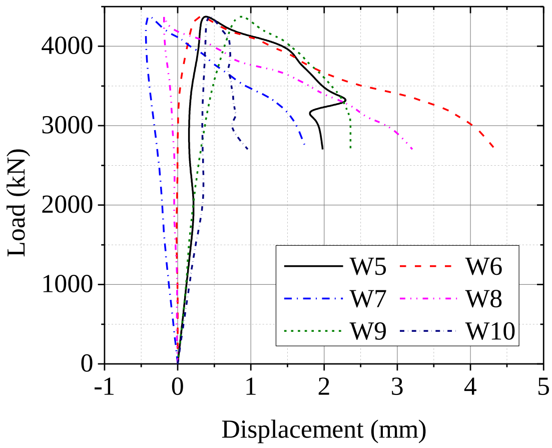

(a) Specimen W-150

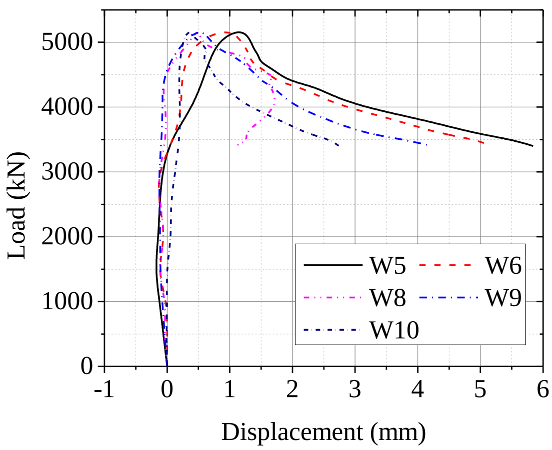

(b) Specimen W-200

Fig. 10 Load-lateral deformation responses

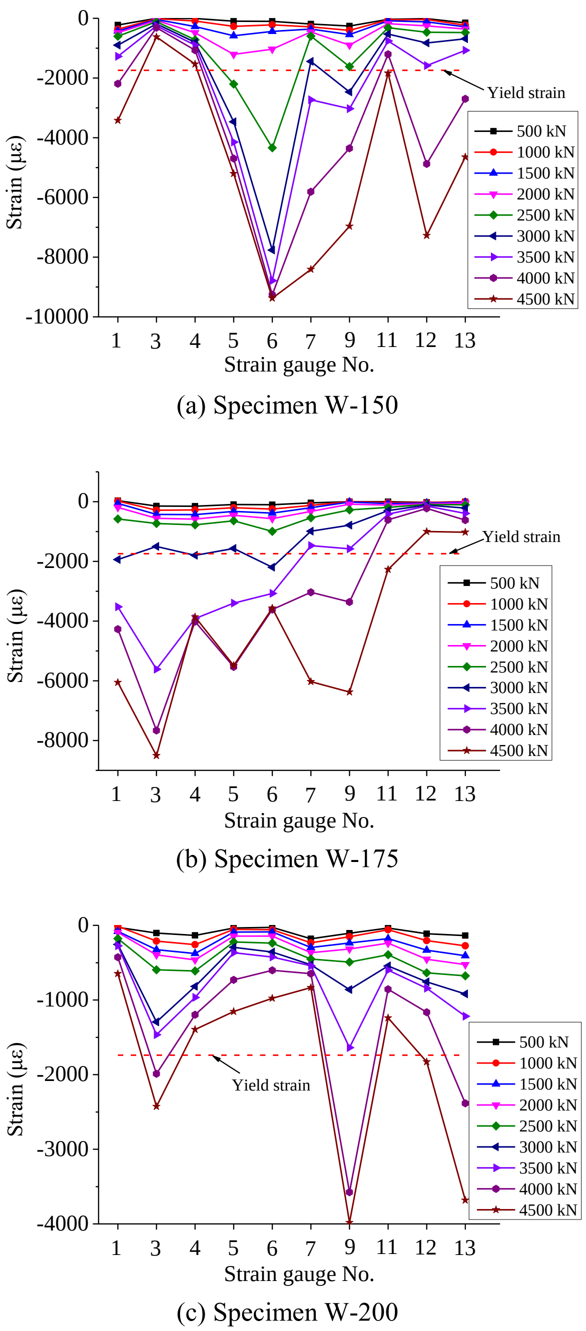

Fig. 11 Strain distribution

Eurocode 4 (EN 1994-1-1, 2004) assumes that the steel plate develops its yield stress of f_y while the concrete core reaches 85% of its compressive strength, as expressed by Eq. (7). CECS 159 (2004) considers to utilize the fully yield strength of steel and fully-developed compressive strength of concrete, as expressed by Eq. (8).

$$N_{AISC}=f_{cr}A_s+0.7f_cA_c \quad (6)$$

$$N_{EC4}=f_yA_s+0.85f_cA_c \quad (7)$$

$$N_{CECS}=f_yA_s+f_cA_c \quad (8)$$

Table 3 Comparison with code-based predictions

Specimen No.	N_{AISC}	N_{EC4}	N_{CECS}	$\frac{N_u}{N_{AISC}}$	$\frac{N_u}{N_{EC4}}$	$\frac{N_u}{N_{CECS}}$
	kN	kN	kN			
W-150	1722	4607	4911	2.61	0.98	0.92
W-175	1979	4979	4979	2.43	0.96	0.90
W-200	2237	5352	5763	2.32	0.97	0.90
Average				2.45	0.97	0.91
Standard deviation				0.120	0.005	0.007

where f_{cr} is the critical buckling stress of steel and can be calculated by Eq. (9) for rectangular filled sections (AISC 360-16 2016).

$$f_{cr}=\frac{9E_s}{(b/t)^2} \quad (9)$$

The predictions by three modern codes are listed in Table 3. It can be seen that AISC 360-16 (2016) significantly underestimates the actual resistance of composite wall under axial compression. The average value and standard deviation of the ratio between test results and predictions by AISC 360-16 are 2.45 and 0.120, respectively. Meanwhile, Eurocode 4 (EN 1994-1-1, 2004) provides the most suitable results, with the average value of 0.97 and standard deviation of 0.005 for the ratio N_u/N_{EC4}. It can be argued that the predictions by Eurocode 4 (EN 1994-1-1, 2004) are slightly unconservative. This may be caused by the fact that in the test, the steel plate reaches its buckling strength rather than yield strength.

5. Conclusions

In this research, the compressive behavior of double skin composite wall with truss connectors was investigated. Axial compressive tests were performed on three specimens with different width-to-thickness ratio. Based on the analysis of test results, the following conclusions are drawn.

(1) The walls fail due to the local buckling of steel plates and crushing of concrete core.

(2) The width-to-thickness ratio does not change the failure mode of the wall, since global buckling was not observed. The increase rate of resistance and initial stiffness is higher than the decrease rate of width-to-thickness ratio, due to the contribution of steel trusses. The strength index is not changed with the varied width-to-thickness ratios. In addition, more uniform strain distribution is found in specimen with smaller width-to-thickness ratio.

(3) The test results are compared with the predictions by AISC 360-16, Eurocode 4, and CECS 159. It is found that AISC 360-16 provides the most conservative results while Eurocode 4 offers the most suitable predictions.

Acknowledgments

This work is sponsored by the Natural Science Foundation of Jiangsu Province (Grant No. BK20170685), and the National Key Research and Development Program of China (Grant No. 2017YFC0703802). The authors would like to thank the Zhejiang Southeast Space Frame Group Company Limited for the supply of test specimens.

References

AISC 360-16 (2016), Specification for structural steel buildings, American Institute of Steel Construction, Chicago, USA.

Asgarian, B., Khazaee, H. and Mirtaheri, M. (2012), "Performance evaluation of different types of steel moment resisting frames subjected to strong ground motion through Incremental dynamic analysis", *Int. J. Steel Struct.*, **12**(3), 363-379. http://dx.doi.org/10.1007/s13296-012-3006-6.

Beiraghi, H. (2018), "Energy demands in reinforced concrete wall piers coupled by buckling restrained braces subjected to near-fault earthquake", *Steel Compos. Struct*., **27**(6), 703-716. http://dx.doi.org/10.12989/scs.2018.27.6.703.

Bruhl J.C. and Varma, A.H. (2017), "Experimental resistance and available ductility of steel-plate composite walls in one-way bending", *J. Struct. Eng.*, **143**(4), 04016222. http://dx.doi.org/10.1061/(ASCE)ST.1943-541X.0001714.

CECS 159 (2004), Technical specification for structures with concrete-filled rectangular steel tube members; China Association for Engineering Construction Standardization, Beijing, China.

Chen, L., Mahmoud, H., Tong, S.M. and Zhou, Y. (2015), "Seismic behavior of double steel plate–HSC composite walls", *Eng. Struct.*, **102**, 1-12. http://dx.doi.org/10.1016/j.engstruct.2015.08.017.

Chen, L.H., Wang, S.Y., Lou, Y. and Xia, D.R. (2019), "Seismic behavior of double-skin composite wall with L-shaped and C-shaped connectors", *J. Constr. Steel Res.*, **160**, 255-270. https://doi.org/10.1016/j.jcsr.2019.05.033.

Choi, B.J., Kang, C.K. and Park, H.Y. (2016), "Strength and behavior of steel plate–concrete wall structures using ordinary and eco-oriented cement concrete under axial compression", *Thin Wall. Struct.*, **84**, 313-324. http://dx.doi.org/10.1016/j.tws.2014.07.008.

Curkovic, I., Skejic, D. and Dzeba, I. (2019), "Seismic performance of steel plate shear walls with variable column flexural stiffness", *Steel Compos. Struct., Int. J.*, **33**(1), 833-850. http://dx.doi.org/10.12989/scs.2019.33.1.833.

Dan, D., Fabian, A. and Stoian, V. (2011), "Nonlinear behavior of composite shear walls with vertical steel encased profiles", *Eng. Struct.*, **33**(10), 2794-2804. http://dx.doi.org/10.1016/j.engstruct.2011.06.004.

Deng, E.F., Zong, L. and Ding, Y. (2019), "Numerical and analytical study on initial stiffness of corrugated steel plate shear walls in modular construction", *Steel Compos. Struct.*, **32**(3), 347-359. http://dx.doi.org/10.12989/scs.2019.32.3.347.

EN 1994-1-1 (2004), Eurocode 4: Design of composite steel and concrete structures-Part 1-1: General rules and rules for buildings, European Standard Institute, Brusels, Belgium.

Eom, T.S., Park, H.G., Lee, C.H., Kim, J.H. and Chang, I.H. (2009), "Behavior of double skin composite wall subjected to in-plane cyclic loading", *J. Struct. Eng.*, **135**(10), 1239-1249. http://dx.doi.org/10.1061/(ASCE)ST.1943-541X.0000057.

Gheidi, M., Mirtaheri, M., Zandi, A.P. and Alanjari, P. (2011), "Effect of filler material on local and global behaviour of buckling-restrained braces", *Struct. Des. Tall Spec. Build.*, **20**(6), 700-710. https://doi.org/10.1002/tal.555.

GB50010-2010 (2010), Code for design of concrete structures; China Architecture & Building Press, Beijing, China.

GB/T 228.1-2010 (2010), Metallic materials-tensile testing-part 1: method of test at room temperature, China Standards Press, Beijing, China.

GB/T 2975-2018 (2018), Steel and steel products-location and preparation of samples and test pieces for mechanical testing, China Standards Press, Beijing, China.

GB/T 50081-2002 (2002), Standard for test method of mechanical properties on ordinary concrete, China Standards Press, Beijing, China.

Hariri-Ardebili, M.A., Rahmani-Samani, H. and Mirtaheri, M. (2014), "Seismic stability assessment of a high-rise concrete tower utilizing endurance time analysis", *Int. J. Struct. Stab. Dyn.*, **14**(6), 1450016. http://dx.doi.org/10.1142/S0219455414500163.

Hilo, S.J., Badaruzzaman, W.H.W., Osman, S.A. and Al-Zand, A.W. (2016), "Structural behavior of composite wall systems strengthened with embedded cold-formed steel tube", *Thin Wall. Struct.*, **98**, 607-616. http://dx.doi.org/10.1016/j.tws.2015.10.028.

Hossain, K.M.A.; Mol, L.K. and Anwar, M.S. (2015), "Axial load behaviour of pierced profiled composite walls with strength enhancement devices", *J. Constr. Steel Res.*, **110**, 48-64. http://dx.doi.org/10.1016/j.jcsr.2015.03.009.

Huang, S.T., Huang, Y.S., He, A., Tang, X.L, Chen, Q.J., Liu, X. and Cai, J. (2018), "Experimental study on seismic behaviour of an innovative composite shear wall", *J. Constr. Steel Res.*, **148**, 165-179. https://doi.org/10.1016/j.jcsr.2018.05.003.

Huang, Z.Y. and Liew, J.Y.R. (2016), "Structural behaviour of steel-concrete-steel sandwich composite wall subjected to compression and end moment", *Thin Wall. Struct.*, **98**, 592-606. http://dx.doi.org/10.1016/j.tws.2015.10.013.

JGJ/T 380-2015 (2015), Technical specification for steel plate shear walls, China Architecture & Building Press, Beijing, China.

Ji, X.D., Cheng, X.W., Jia, X.F. and Varma, A.H. (2017), "Cyclic in-plane shear behavior of double-skin composite walls in high-rise buildings", *J. Struct. Eng.*, **143**(6), 04017025. https://doi.org/10.1061/(ASCE)ST.1943-541X.0001749.

Karami-Mohammadi, R., Mirtaheri, M., Salkhordeh, M., Mosaffa, E., Mahdavi, G. and Hariri-Ardebili, M. (2019), "Seismic mitigation of substation cable connected equipment using friction pendulum systems", *Struct. Eng. Mech.*, **72** (6), 805-816. https://doi.org/10.12989/sem.2019.72.6.805.

Leekitwattana, M., Boyd, S.W. and Shenoi, R.A. (2011), "Evaluation of the transverse shear stiffness of a steel bi-directional corrugated-strip-core sandwich beam", *J. Constr. Steel Res.*, **67**(2), 248-254. https://doi.org/10.1016/j.jcsr.2010.07.010.

Li, D., Smith, S. and Ma, X. (2016), "End condition effect on initial buckling performance of thin plates resting on tensionless elastic or rigid foundations", *Int. J. Mech. Sci.*, **105**, 83-89. https://doi.org/10.1016/j.ijmecsci.2015.11.001.

Liu, W.Y., Li, G.Q. and Jiang, J. (2018), "Capacity design of boundary elements of beam-connected buckling restrained steel plate shear wall", *Steel Compos. Struct*., **29**(2), 231-242. https://doi.org/10.12989/scs.2018.29.2.231.

Luo, Y.F., Guo, X.N., Li, J., Xiong, Z., Meng, L., Dong, N. and Zhang, J. (2015), "Experimental research on seismic behaviour of the concrete-filled double-steel-plate composite wall", *Adv. Struct. Eng.*, **18**(11), 1845-1858. http://dx.doi.org/10.1260/1369-4332.18.11.1845.

McKinley, B. and Boswell, L.F. (2002), "Behaviour of double skin composite construction", *J. Constr. Steel Res.*, **58**(10), 1347-1359. https://doi.org/10.1016/S0143-974X(02)00015-9.

Mirtaheri, M., Gheidi, A., Zandi, A.P., Alanjari, P. and Samani, H.R. (2011), "Experimental optimization studies on steel core lengths in buckling restrained braces", *J. Constr. Steel Res.*, **67**(8), 1244-1253. https://doi.org/10.1016/j.jcsr.2011.03.004.

Mirtaheri, M., Sehat, S. and Nazeryan, M. (2018), "Improving the behavior of buckling restrained braces through obtaining optimum steel core length", *Struct. Eng. Mech.*, **65**(4), 401-408. https://doi.org/10.12989/sem.2018.65.4.401.

Mydin, M.A.O. and Wang, Y.C. (2011), "Structural performance of lightweight steel-foamed concrete-steel composite walling system under compression", *Thin Wall. Struct.*, **49**, 66-76. http://dx.doi.org/10.1016/j.tws.2010.08.007.

Nguyen, N.H. and Whittaker, A.S. (2017), "Numerical modelling of steel-plate concrete composite shear walls", *Eng. Struct.*, **150**, 1-11. http://dx.doi.org/10.1016/j.engstruct.2017.06.030.

Nie, J.G., Hu, H.S., Fan, J.S., Tao, M.X., Li, S.Y. and Liu, F.J. (2013), "Experimental study on seismic behavior of high-strength concrete filled double-steel-plate composite walls", *J. Constr. Steel Res.*, **88**, 206-219. http://dx.doi.org/10.1016/j.jcsr.2013.05.001.

Prabha, P., Marimuthu, V., Saravanan, M., Palani, G.S., Lakshmanan, N. and Senthil, R. (2013), "Effect of confinement on steel-concrete composite light-weight load-bearing wall panels under compression", *J. Constr. Steel Res.*, **81**, 11-19. http://dx.doi.org/10.1016/j.jcsr.2012.10.008.

Qin, Y., Shu, G.P., Zhou, G.G. and Han, J.H. (2019a), "Compressive behavior of double skin composite wall with different plate thicknesses", *J. Constr. Steel Res.*, **157**, 297-313. https://doi.org/10.1016/j.jcsr.2019.02.023.

Qin, Y., Shu, G.P., Zhou, X.L., Han, J.H. and He, Y.F. (2019b), "Height-thickness ratio on axial behavior of composite wall with truss connector", *Steel Compos. Struct.*, **30**(4), 315-325. https://doi.org/10.12989/scs.2019.30.4.315.

Qin, Y., Chen, X., Xi, W., Zhu, X.Y. and Chen, Y.Z. (2020a), "Compressive behavior of rectangular sandwich composite wall with different truss spacings", *Steel Comp. Struct.*, **34**(6), 783-794. https://doi.org/10.12989/scs.2020.35.4.495.

Qin, Y., Chen, X., Zhu, X.Y., Xi, W. and Chen, Y.Z. (2020b), "Structural behavior of sandwich composite wall with truss connectors under compression", *Steel Compos. Struct.*, **35**(2), 159-169. https://doi.org/10.12989/scs.2020.35.2.159.

Ridha, M.M., Li, D., Clifton, G.C. and Ma, X. (2019), "Structural behavior of composite panels made of lightly profiled steel skins and lightweight concrete under concentric and eccentric loads", *J. Struct. Eng.*, **145**(10), 1-9. https://doi.org/10.1061/(ASCE)ST.1943-541X.0002380.

Samani, H.R., Mirtaheri, M., Zandi, A.P. and Bahai, H. (2014), "The effects of dynamic loading on hysteretic behavior of frictional dampers", *J. Shock Vib.*, 181534. https://doi.org/10.1155/2014/181534.

Samani, H.R., Mirtaheri, M. and Rafiee, M. (2015), "The effects of various slippage loads on the response modification factor of steel structures equipped with frictional dampers", *Int. J. Struct. Stab. Dyn.*, **15**(6), 1450080. https://doi.org/10.1142/S0219455414500801.

Seddighi, M., Barkhordari, M.A. and Hosseinzadeh, S.A.A. (2019), "Behavior of FRP-reinforced steel plate shear walls with various reinforcement designs", *Steel Compos. Struct.*, **33**(5), 729-746. http://dx.doi.org/10.12989/scs.2019.33.5.729.

Shariati, M., Faegh, S.S., Mehrabi, P., Bahavarnia, S., Zandi, Y., Masoom, D.R., Toghroli, A., Trung, N.T. and Salih, M.N.A. (2019), "Numerical study on the structural performance of corrugated low yield point steel plate shear walls with circular openings", *Steel Compos. Struct.*, **33**(4), 569-581. http://dx.doi.org/10.12989/scs.2019.33.4.569.

Wright, H. (1998), "The axial load behaviour of composite walling", *J. Constr. Steel Res.*, **45**(3), 353-375. https://doi.org/10.1016/S0143-974X(97)00030-8.

Yan, J.B., Wang, Z., Wang, T. and Wang, X.T. (2018), "Shear and tensile behaviors of headed stud connectors in double skin composite shear wall", *Steel Compos. Struct.*, **26**(6), 759-769. https://doi.org/10.12989/scs.2013.91.4.1301.

Yan, J.B., Chen, A.Z. and Wang, T. (2019), "Developments of double skin composite walls using novel enhanced C-channel connectors", *Steel Compos. Struct.*, **33**(6), 877-889. https://doi.org/10.12989/scs.2019.33.6.877.

Yang, Y., Liu, J.B. and Fan, J.S. (2016), "Buckling behavior of double-skin composite walls: An experimental and modeling study", *J. Constr. Steel Res.*, **121**, 126-135. http://dx.doi.org/10.1016/j.jcsr.2016.01.019.

CC